Numerical and Experimental Investigating on Adhesive Joint Parts for Crash Applications

G. Kirov[1], F. Grabner[1], B. Fellner[2], E. Mukeli[3], Z. Khalil[1]

[1]Leichmetallkompetenzzentrum Ranshofen GmbH
[2]Magna Steyr Engineering AG & Co KG
[3]Magna Steyr Fahrzeugtechnik AG & Co KG

Abstract

Aluminum profiles joined by adhesive bonds are well-established in the production of modern car bodies. However, the influence of the base material on the failure behavior of the adhesive has not yet been clearly investigated. The objective of this paper is to describe the influence of the adhesive on the deformation of aluminum parts under different car crash conditions by using multiple experiments and numerical methods.
A strain-rate dependent cohesive model in LS-DYNA was used to describe the material characteristics of EN AW-6xxx aluminum profiles and the adhesive Betamate Parameter finding was conducted both by quasi static and dynamic tests and by reverse engineering. In order to obtain mechanical material parameters for the models experimental testing of bonded specimens was performed. The strain-rate dependent behavior of the adhesive was investigated by testing at different speeds and different load directions (normal and shear). Furthermore, the numerical model was verified on a simplified T-pillar part.
The results show that the strain-rate dependency of the adhesive influences the deformation behavior of the aluminum parts. These findings may contribute to the improvement of passenger safety.

1 Introduction

Different materials are combined in a car body to increase the light weight potential of the design. Therefore, joining techniques are relevant regarding crash safety. For the simulation of adhesive bonds different cohesive material models in LS-DYNA are available [1]. Commonly used cohesive models include models for the rate dependent effect of the adhesive bond and changing material properties depending on the deformation rate [2][3][4].
In this work investigations of the strain rate dependence ($\dot{\varepsilon}$ = *(dε/dt)*) were made using the cohesive model "MAT_COHESIVE_MIXED-MODE_ELASTOPLASTIV_RATE" ("MAT_240") [1]. The failure behavior in this material model can be described by normal and shear load direction *Fig. 1*. Therefore, the strain rate dependency in the normal direction is given by the stress value $T(\dot{\varepsilon}_{eq})$ and the energy release rate $GIC(\dot{\varepsilon}_{eq})$ .The strain rate dependency in shear direction is given by the stress value $S(\dot{\varepsilon}_{eq})$ and the energy release rate $GIIC(\dot{\varepsilon}_{eq})$.

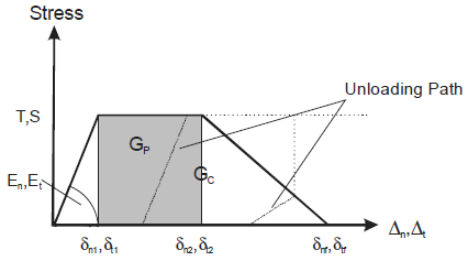

Fig. 1: Schematic of the separation law for normal and shear direction of MAT_240 [1].

The stress value $T(\dot{\varepsilon}_{eq})$can be described by a quadratic logarithmic (2.1) or by a linear logarithmic (2.2) functional approach of *EDOT_T*.

$$T(\varepsilon_{eq}) = |T0| + |T1|\left\langle \ln\frac{\dot{\varepsilon}_{eq}}{EDOT\_T}\right\rangle^2$$ for mode I when *T0*< 0 and *T1*>0, (1.1)

$$T(\dot{\varepsilon}_{eq}) = |T0| + |T1|\left\langle \ln \frac{\dot{\varepsilon}_{eq}}{EDOT\_T} \right\rangle$$ for mode I when T0> 0 and T1<0, (1.2)

The shear stress value $S(\dot{\varepsilon}_{eq})$ and can be described by quadratic logarithmic (2.3) or by linear logarithmic (2.4) functional approach of *EDOT_S.*

$$S(\dot{\varepsilon}_{eq}) = |S0| + |S1|\left\langle \ln \frac{\dot{\varepsilon}_{eq}}{EDOT\_S} \right\rangle^2$$ for mode II when *S0*< 0 and *S1*>0, (1.3)

$$S(\dot{\varepsilon}_{eq}) = |S0| + |S1|\left\langle \ln \frac{\dot{\varepsilon}_{eq}}{EDOT\_S} \right\rangle$$ for mode II when T0> 0 and T1<0, (1.4)

To describe the strain rate dependency of the energy release rates ($GIC(\dot{\varepsilon}_{eq})$ $GIIC(\dot{\varepsilon}_{eq})$) the lower (*G1C_0*, *G2C_0)* and upper bound (*G1C_INF, G2C_INF)* are needed as well as *EDOT_G1* and *EDOT_G2.*

$$G_{IC}(\dot{\varepsilon}_{eq}) = |G1C\_0| + \left(G1C\_INF - |G1C\_0|\right)\exp\left(-\frac{EDOT\_G1}{\dot{\varepsilon}_{eq}}\right)$$ for mode I (1.5)

$$G_{IIC}(\dot{\varepsilon}_{eq}) = |G2C\_0| + \left(G2C\_INF - |G2C\_0|\right)\exp\left(-\frac{EDOT\_G2}{\dot{\varepsilon}_{eq}}\right)$$ for mode II (1.6)

The failure behaviour in mixed mode (see *Fig. 2*) is a combination of normal and shear direction which are coupled by the angel γ. Here the maximum displacement δ_{mf} is calculated by 2.7. More detailed information about MAT_240 is given in the LS-DYNA manual [1].

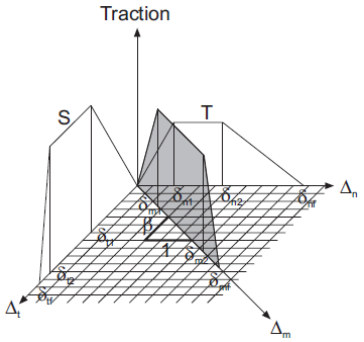

Fig. 2: Schematic of the separation law for mixed mode direction of MAT_240 [1].

$$\delta_{mf} = \frac{\delta_{m1}(\delta_{m1} - \delta_{m2})E_n G_{IIC}\cos^2\gamma + G_{IC}\left(2G_{IIC} + \delta_{m1}(\delta_{m1} - \delta_{m2})E_t \sin^2\gamma\right)}{\delta_{m1}\left(E_n G_{IIC}\cos^2\gamma + E_t G_{IC}\sin^2\gamma\right)}$$ (1.7)

It is essential identifying the mentioned parameters, for setting up the MAT_240 model. Therefore different experimental tests and numerical simulations are conducted to obtain these parameters [2][3][5][6][7]. Determining parameters for rate dependency is rater complex due to different testing velocities and various specimens' geometries. To gather information of the adhesive material properties the influence of the base material's plastic deformation should be excluded. The *IFAM institute Bremen* therefore developed the "Tapered Double Cantilever Beam (TDCB)" test and the "Tapered End-Notched (TENF)" test [2]. In this test the geometry and the steel material of the samples assure that no plastic deformation effects interfere with the parameter measurement for the adhesive. Betamate has been widely investigated so there is significant data is available [2][3][4][6][7][8].

A general opinion is that in the case of cohesive failure the parameter identification is independent of the base material (steel or aluminum). Therefore, in this work the Betamate parameters measured on steel specimens have been used for aluminum EN AW 6xxx bonded parts.

The validation of the adhesive material model was made from the simple sample level up to simple part level. Thus, static and dynamic tests were carried out to investigate the influence of the adhesive joints on the deformation behavior. For testing under dynamic conditions on the part level a pendulum impact test was constructed. In the case of the adhesive joints the rate-dependent effects were investigated by experimental and numerical methods.

2 Experiments and simulation

2.1 Experiments simple sample level

The adhesive was characterized with static and dynamic tests at the IFAM institute Bremen. Samples were made to evaluate the two dominant loading directions. For the normal direction DCB specimens were used [10] and for shear lap-shear tension specimens were used.
Fig. 3 a shows a schematic of the DCB test specimen. To reduce effects which influence the test results an initial crack was introduced to the beginning of the sample using PTFE film. All adhesive layers of Betamate had a thickness of 0.3 *mm*. *Fig. 3* b-d shows the characteristic cohesive failure behavior observed for the DCB tests. These tests were done with a crosshead speed of 0.5 *mm/s* (*Fig. 3* b), *5 mm/s* (*Fig. 3* c), and 500 *mm/s* (*Fig. 3* d).

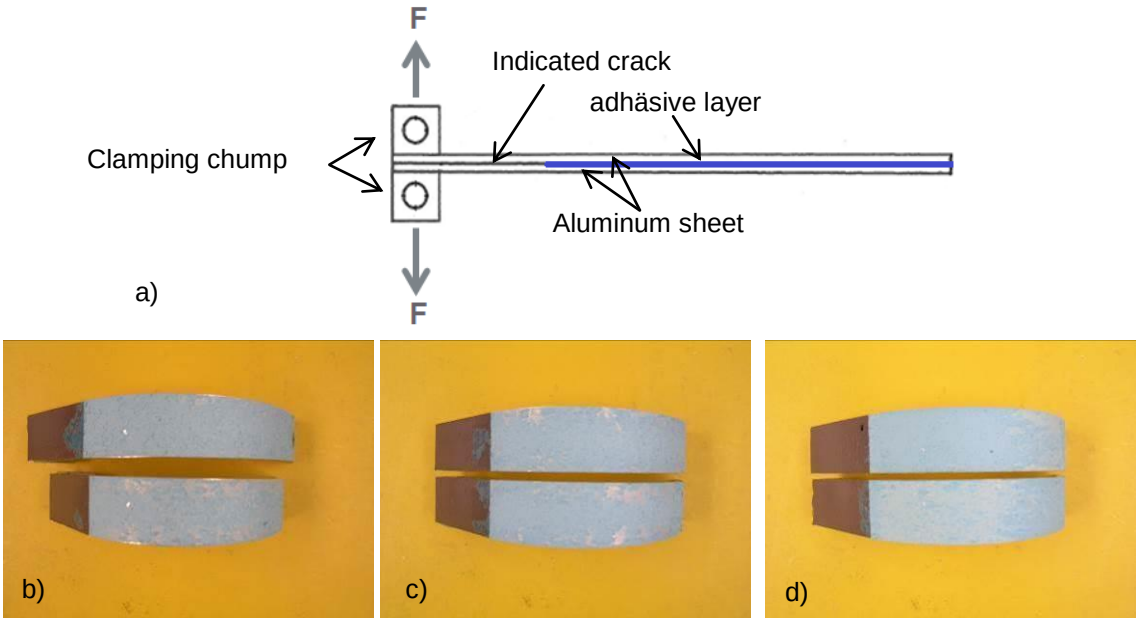

Fig. 3: Schematic of the BCD test specimens (a) and results from the DCB test for mode I (b-d). Visible is the (broken) adhesive layer and the PTFE-film; b) characteristic failure behavior for 0,5 mm/s, c) characteristic failure behavior for 5 mm/s, d) characteristic failure behavior for 500 mm/s.

In these tests force displacement curves were measured (*Fig. 4*). The results show a changing of the force level depending on the testing speed. This can be interpreted as a strain rate dependency of the Betamate adhesive in the normal direction.

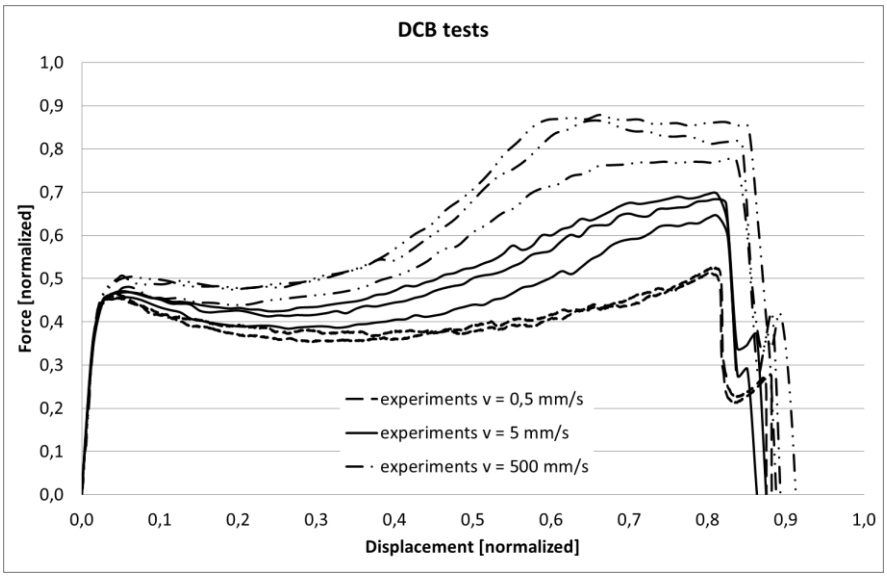

Fig. 4: Force displacement results for DCB test done by 0,5 mm/s, 5 mm/s and 500 mm/s.

The lap-shear tension tests were carried out at the same test speeds as for the DCB test. *Fig. 5* a shows the schematic lap-shear tension specimen. Similar to the DCB test specimens the lap-shear tension specimens were also prepared with an adhesive layer of 0,3 mm. The experiments were dominated by cohesive failure mode and this can be seen in *Fig. 5* b-d

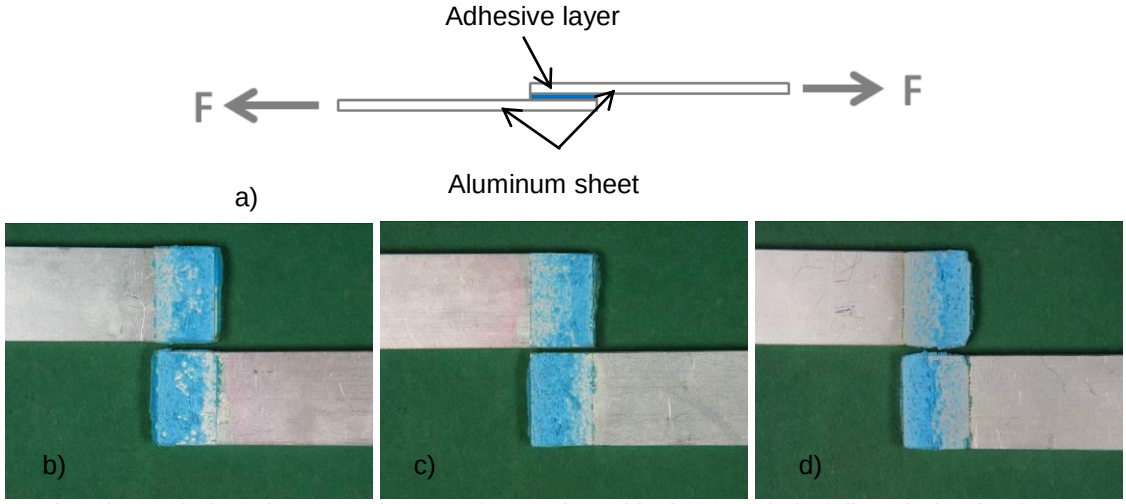

Fig. 5: a) Schematic lap-shear tension test for mode II, b) characteristic failure behavior for 0,5 mm/s, c) characteristic failure behavior for 5 mm/s, d) characteristic failure behavior for 500 mm/s.

As before, force-displacement curves were generated from these tests (*Fig. 6*). Similar to the results from the DCB tests there is a change in the force and in the maximum displacement depending on the testing speed. This can be interpreted as a strain rate dependency of the Betamate adhesive in lap-shear tension direction.

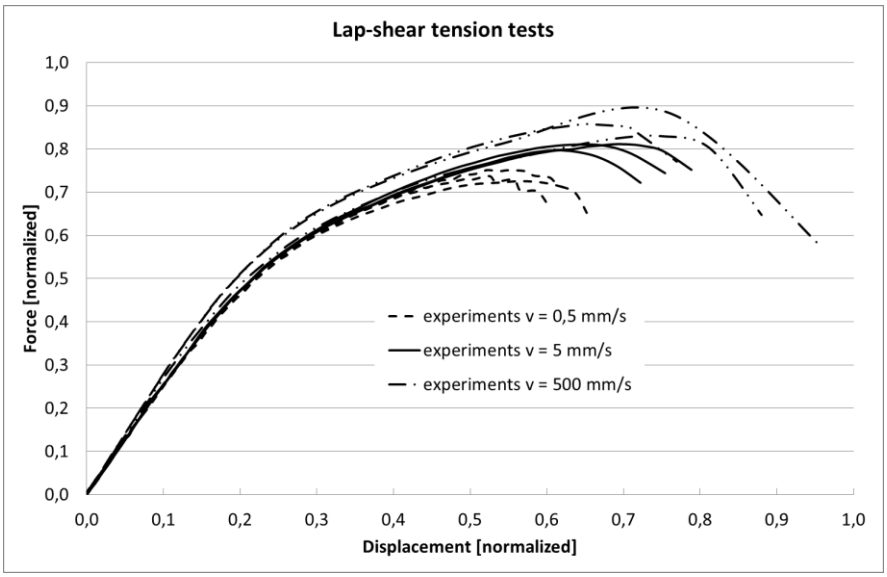

Fig. 6: Force displacement results for lap-shear tension tests made for 0,5 mm/s, 5 mm/s and 500 mm/s.

2.2 Simulation of the simple sample

Based on the experiments numerical models were built up as can be seen in *Fig. 7* and *Fig. 8*. Here an element size of 1 mm was used for the aluminium part. To consider the plastic deformation of the EN AW 6xxx parts the LS-Dyna material card *MAT_PIECEWISE_LINEAR_PLASTICITY was used. The adhesive layer was based on the experiments with a modeled thickness of 0.3 *mm*. The measurement of the force and displacement was similar to the experiments and was made to test the adhesive area in both models.

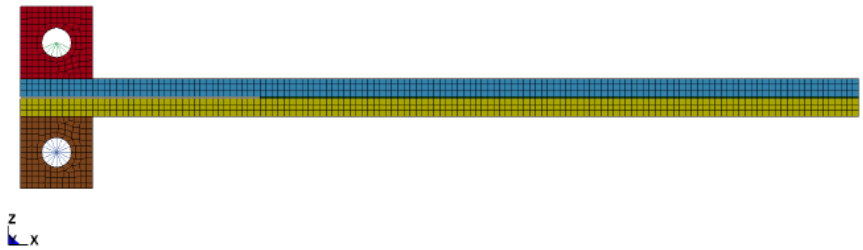

Fig. 7: Schematic mesh model of DCB-test.

Fig. 8: Schematic mesh model of lap-shear tension test.

The simulations of DCB tests and lap-shear tension tests were made with different cohesive MAT_240 cards. Based on the research work of IFAM – Bremen in the Fost project [2] and the experimental test results two cards, a quasi static and a dynamic card, were created. A second set of a static and dynamic cards were created by LKR. This was done with the help of the data provided by IFAM and through reverse engineering using the optimization tool LS-OPT.
Table 1 shows the normalized parameters used and some differences in the values of the cards can be seen. The big differences for quasi static velocities are given by the tension (T) value and the shear modulus (GMOD). For the dynamic cards, great deviations are given by the tension (T), shear (S) values and the energy release rates (GIIC).

Parameter from literature [2]			Modified card for aluminum specimen		
	parameter	data		parameter	data
L_MAT_240 quasi static	EMOD	0,95	M_ MAT_240 quasi static	EMOD	1,00
	T	0,22		T	0,39
	GIC	0,72		GIC	0,73
	GMOD	1,00		GMOD	0,25
	S	0,71		S	0,64
	GIIC	0,70		GIIC	1,00
L_MAT_240 dynamic	EMOD	0,95	M_ MAT_240 dynamic	EMOD	1,00
	T	0,89		T	1,00
	GIC	1,00		GIC	0,89
	GMOD	1,00		GMOD	0,25
	S	1,00		S	0,65
	GIIC	0,70		GIIC	0,94

Table 1: Quasi static and dynamic normalized parameter set of MAT_240 used for the simulation.

Fig. 9 shows the comparison of the DCB experiments with the simulation work. In the left graph the results of the two quasi static MAT_240 cards are shown. Here both MAT_240 cards show a higher peak in the force level at the beginning compared to the experiments. It is also clear the simulation of the L_MAT_ quasi static card ends at a lower force. However, the total failure displacement of both simulations correlates to the experiments. A characteristic behavior of the DCB test for aluminum specimens is a decreasing force after the first force peak. This depends on the plastic deformation of the aluminum sheets and can be seen in both simulations. The M_MAT_240 quasi static card can describe this behavior in a better agreement to the experiments.
In the right graph the experiments and the simulation results at a speed of 500 mm/s are given. Here, two dynamic MAT_240 cards and the M_MAT_240 rate card are used to describe the failure behavior of the DCB tests. All simulations overestimate the initial force peak. After the first peak the force is constant up to a certain point where it starts to rise again before reaching a plateau. This behavior is described by the simulation, so all simulations here show a good correlation to the experiments. Only some differences on the force can be seen. Since the M_MAT_240 rate card includes the local strain rate this result shows that considering the local strain rate in the calculation is important.

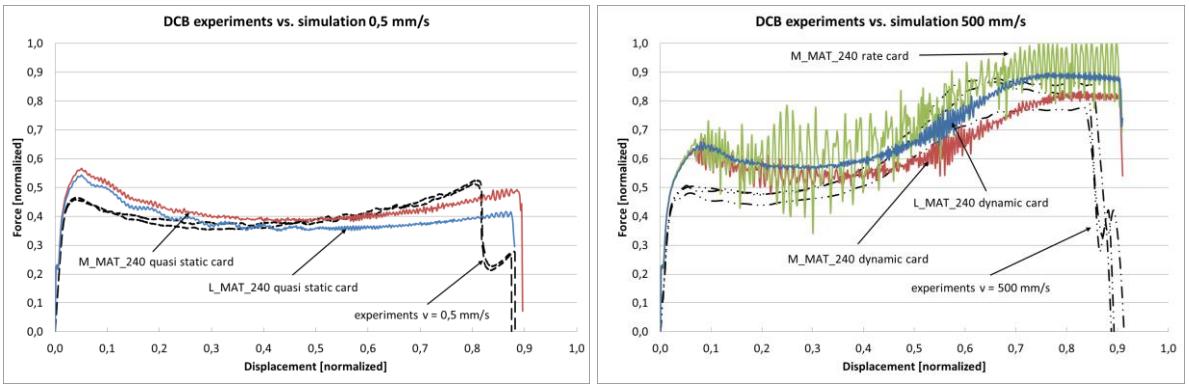

Fig. 9: Comparison of DCB experiments vs. simulation left: 0,5 mm/s, right: 500 mm/s.

The results of the shear tension experiments and simulations are given in *Fig. 10*. Both simulations made at 0,5 mm/s generate a higher force than measured in the experiments. Here the plastic deformation of the specimen and the failure behavior of the adhesive from the simulation cannot match the same characteristic from the experiments. The simulation from the L_MAT_240 quasi static card shows a higher force but a lower displacement compared to the simulation done with the M_MAT_240 quasi static card. This is an effect of the differences of the parameters S and GIIC.
The simulation of the dynamic lap-shear tension test was done with the help of two dynamic MAT_240 cards and the M_MAT_240 rate card. Here, differences between the simulation and the experiments can be seen. Both modified cards show a good correlation to the experiments. Here the M_MAT_240 rate card gives a lower maximum force level compared to the M_MAT_240 dynamic card. Here, a strain rate effect is given which behaves slightly different compared to M_MAT_240 dynamic card. The simulation done with the L_MAT_240 dynamic card cannot describe the same characteristic as the experiments. Additionally, the higher shear stress value S (*Table 1*) results in a higher plastic deformation of the specimen and a higher displacement.

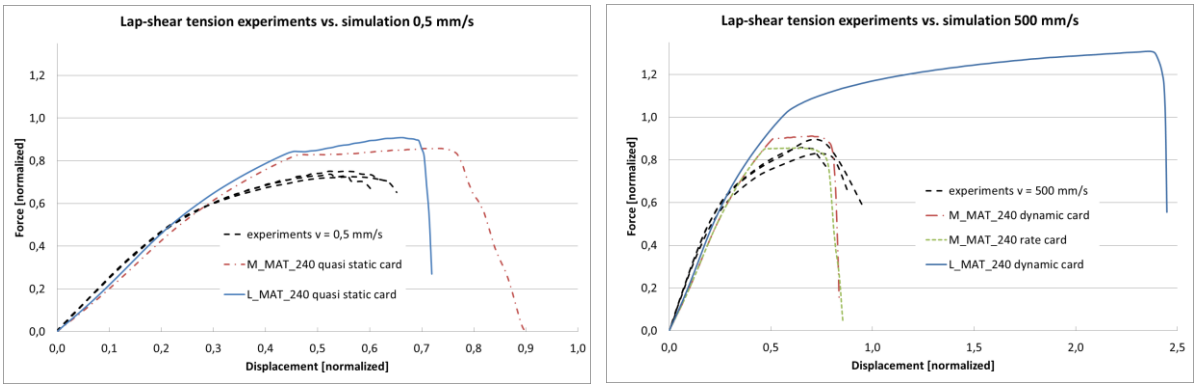

Fig. 10: Comparison of lap-shear tension experiments vs. simulation left: 0,5 mm/s, right: 500 mm/s.

2.3 Experiments and simulation on the simple part

For a more realistic verification of the different dynamic MAT_240 cards pendulum tests were carried out on a simple joined T-pillar part. Here EN AW 6xxx profiles of 50 mm x 50 mm were joined with EN AW 6xxx angle and cover plates. The adhesive area was 25 mm x 50 mm.
0 shows the test setup for the impact tests. A maximum speed of 30 km/h was possible for this test. . Adhesive joined specimens were tested with an impacting speed of 15 km/h and 30 km/h and force-time data of the impacting device was recorded.

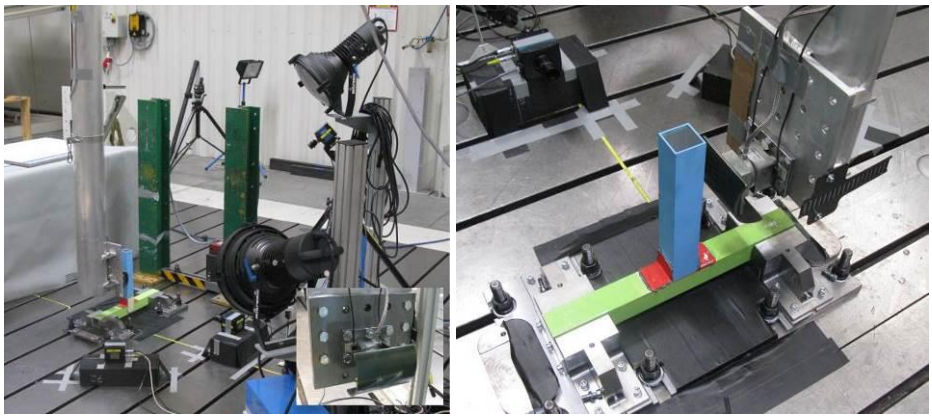

Fig. 11: Test setup for dynamic tests on the T-pillar, b) detail of the T-pillar and impactor for the dynamic tests.

Numerical models were created based on these experiments. *Fig. 12* shows the mesh model used for the simulation. Here a shell mesh of 3 mm was used to build the T-pillar. The joined areas of adhesive have been modelled with solid elements of 3x3x3 mm, as can be seen in *Fig. 13* a and *Fig. 13* b. And, the real thickness of the adhesive layer (0.3 mm) was defined in the MAT_240 card. The simulation was made using the L_MAT_240 dynamic card and the M_MAT_240 rate card so that the rate-dependent effects were included. A *MAT_PIECEWISE_LINEAR_PLASTICITY card with a simple failure criteria was used to describe the crack initiation of the cover plate. For the comparison between experiments and simulation the same time step from the experimental data and a CFC600 filter were used.

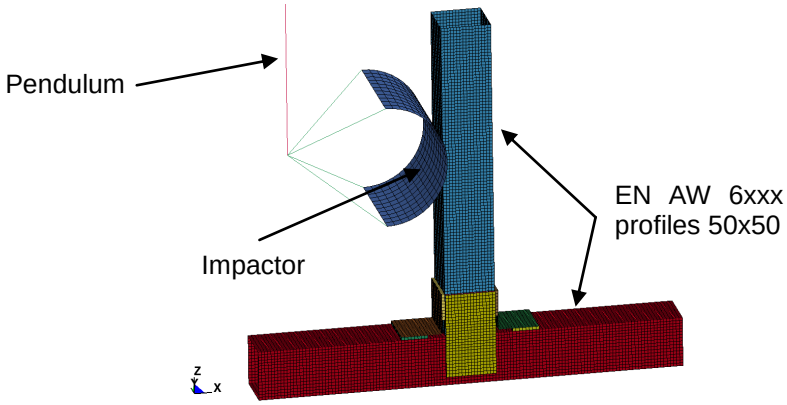

Fig. 12: Mesh model of impact test for the T-pillar simulation.

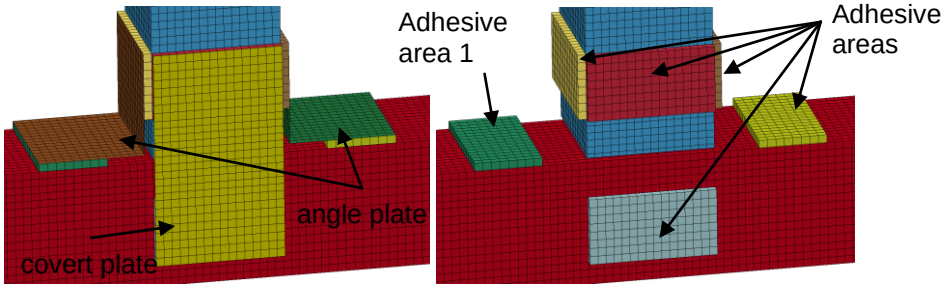

Fig. 13: a) Detail mesh modeling of EN AW 6xxx angle and cover plate and adhesive; b) detail of the mesh modeling of adhesive layer.

Fig. 14 shows the results for force-time data of the experiments and simulation for an impact velocity of 15 km/h. The results in the charts can be divided into two areas. From 0 to 0,013 s where primarily the failure of adhesive is dominating and form 0,013 s to the end where failure occurs in the aluminum sheets. The black lines are the results from the experiment, the blue dashed line is the simulation made with the L_MAT_240 dynamic card and the orange dashed-dotted line is the simulation made with the M_MAT_240 rate card. In the first view the results between the simulation and the experiment correlate in a good way. Both simulations show a little higher force peak at the beginning up to 0,005

s. The simulation done with the M_MAT_240 rate card indicates a higher force peek at 0,013 s and highlights the end of the adhesive failure on area 1.
In the detailed view of the failure behavior in the adhesive area (*Fig. 16* to *Fig. 18*), differences in the simulation and the experiments can be observed. In 0 the total failure of the adhesive in area 1 ends and the first crack initiation on the cover plate occurs by 0,013 s. The simulation done by the L_MAT_240 dynamic card shows in *Fig. 16* a partial failure of the adhesive surface and a first crack initiation on the cover plate by 0,0094 s. Total failure of the adhesive area 1 ends at 0,011 s (see *Fig. 17*) and this does not correlate exactly to the experiments. *Fig. 18* shows the simulation done with the modified rate dependent MAT_240 card. Here the total failure of the adhesive area 1 and the first crack initiation of the covert plate are complete at 0,012 s and is a good agreement with the experiments.

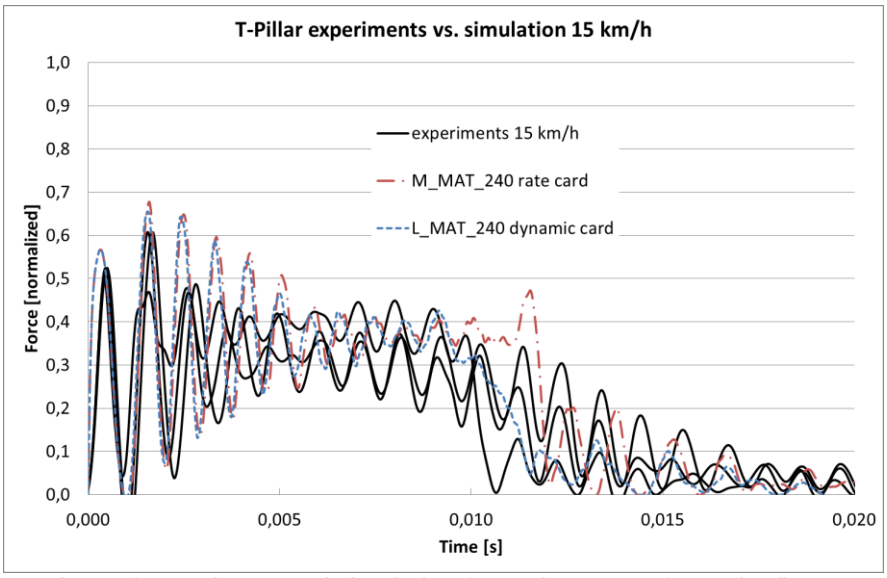

Fig. 14: a) Comparison of experiment and simulation force-time curve for 15 km/h.

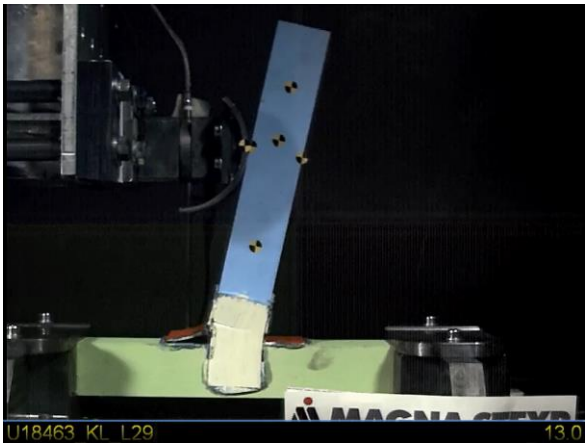

Fig. 15: Experiment of adhesive joined T-pillar with impact velocity of 15 km/h. Total failure of adhesive surface and first crack initiation on cover plate at 0,013 s.

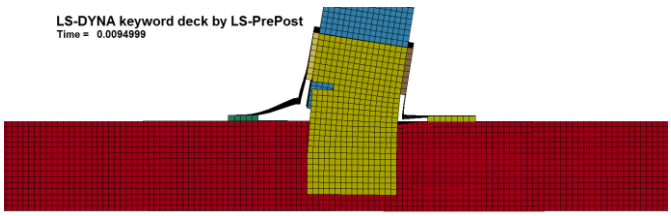

Fig. 16: Simulation with L_MAT_240 dynamic card of adhesive joined T-pillar with impact velocity of 15 km/h. Partial failure of adhesive surface and first crack initiation on cover plate by 0,0094 s.

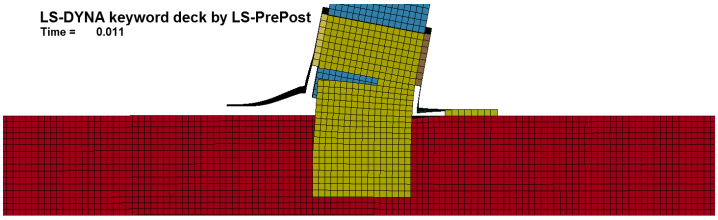

Fig. 17: Simulation with L_MAT_240 dynamic card of adhesive joined T-pillar with impact velocity of 15 km/h. Total failure of adhesive surface by 0,011 s.

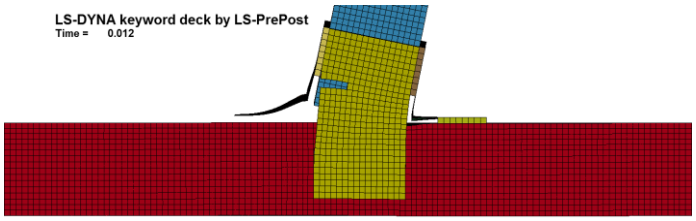

Fig. 18: Simulation with M_MAT_240 rate card of adhesive joined T-pillar with impact velocity of 15 km/h total. Failure of adhesive surface and first crack initiation on cover plate by 0,012 s.

The following figures show the results from the experiments and simulation of the T-pillar for the impact velocity of 30 km/h. *Fig. 19* compares the force time curves from the experiments and simulation. Here the results can also be divided into two areas; from 0 to 0,007 s where primarily failure of the adhesive is dominating and form 0,007 s to the end were failure occurs in the cover aluminum sheet. Both simulations indicate a higher force peak than measured in the experiments over the first area (0 to 0,007 s). After 0,007 s the force calculated in the simulations is similar to the experimental results. In the detailed view of experiment and simulation (*Fig. 20* to *Fig. 23*) the failure behavior of the adhesive layer in area 1 and the crack initiation on the cover plate can be seen. The experiment shows in *Fig. 20* a total failure of the adhesive area 1 and the first crack initiation on the cover plate at 0,007 s. *Fig. 21* highlights the simulation made with the L_MAT_240 dynamic card. Here the partial failure of adhesive area 1 and first crack initiation on cover plate are done by 0,0049 s. The total failure of adhesive area 1 can be seen by 0,0059 s (*Fig. 22*). In comparison to the experiments the first crack initiation and the total adhesive failure of area 1 from the simulation starts at an earlier time.
Fig. 23 shows the results of the simulation made with the modified rate dependent MAT_240 card. Here, the total failure of the adhesive area 1 and the first crack initiation of the cover plate at 0,007 s are similar to the experiment and is a good match.

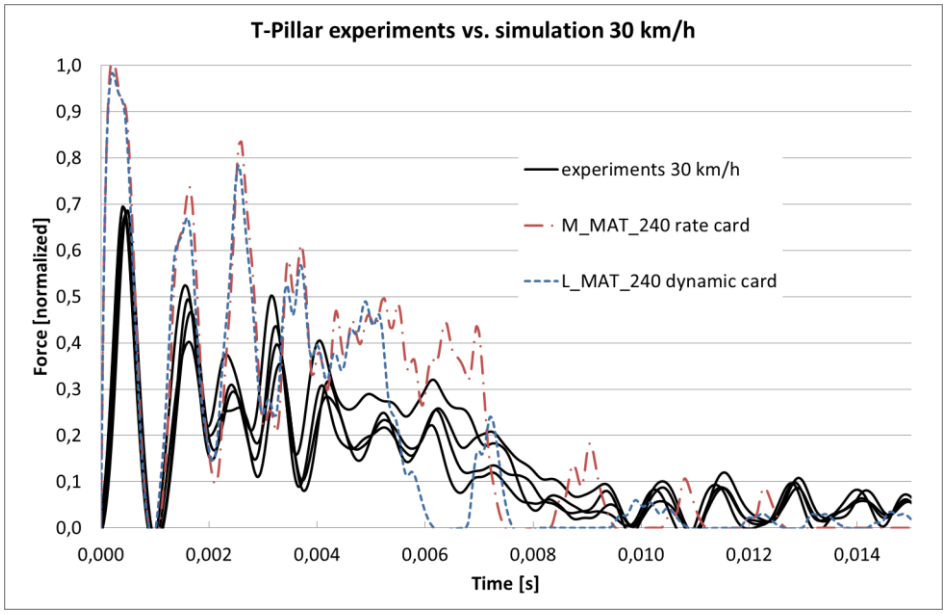

Fig. 19: Comparison of experiment and simulation force-time curve by 30 km/h.

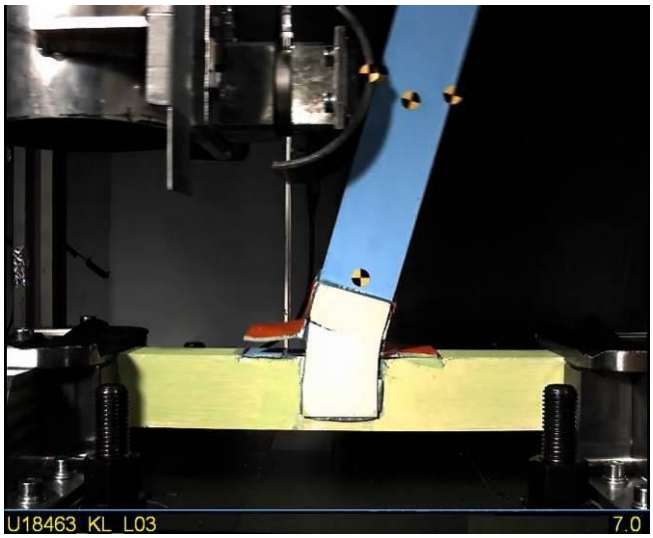

Fig. 20: Experiment of adhesive joined T-pillar with impact velocity of 30 km/h. Total failure of adhesive surface and first crack initiation on cover plate by 0,007 s.

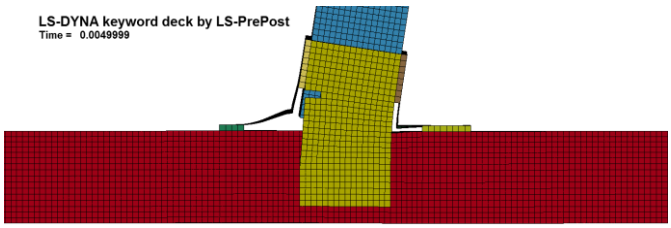

Fig. 21: Simulation with L_MAT_240 dynamic card of adhesive joined T-pillar with impact velocity of 30 km/h. Partial failure of adhesive surface and first crack initiation on cover plate by 0,0049 s.

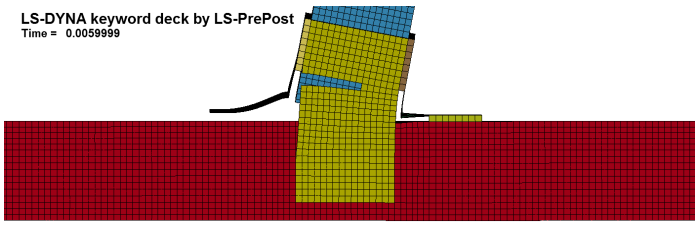

Fig. 22: Simulation with L_MAT_240 dynamic card of adhesive joined T-pillar with impact velocity of 30 km/h. Total failure of adhesive surface by 0,0059 s.

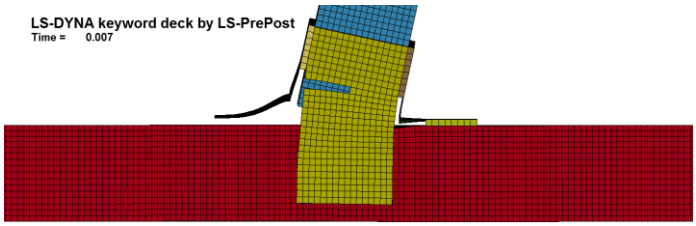

Fig. 23: Simulation with M_MAT_240 rate card of adhesive joined T-pillar with impact velocity of 30 km/h. Total failure of adhesive surface and first crack initiation on cover plate by 0,007 s.

3 Summary

This work showed different methods to determine the material parameter for cohesive models; in this case for MAT_240. One highlight was that the parameter identification is dependent on the base material. So, parameter identification needs to be made on the bonded material, as made here for aluminum. The experimental work also shows a strain rate dependency of the Betamate, and this can be represented in the simulation work by the MAT_240. Therefore, the simulations carried out with this model show a very good correlation with the dynamic experiments.

The experiments show an influence of the base material on the failure behavior of the adhesive and provide needed information for joining different materials, such as steel and aluminum. This understanding is needed to design crash relevant parts with a good crash performance and the outcome of this work contributes directly to car safety. These results can be scaled to full car bodies to realize the needed crash performance.
The work also shows that a deep understanding of experimental testing and a numerical description of adhesive joints is needed to describe in detail the failure characteristic of bonded parts. Therefore, for different used base materials the respective parameter fitting needs to be done. In this work the experimental testing for identifying the needed model parameters revealed that standard test routines were missing. When the standards become available cohesive material cards could be identified in a short time with high quality. For the future, investigations are needed to create standard tests for the characterization of joints. Also, these standard tests could be used to set up a material data bank for joining parameters.

4 Literature

[1] J.O. Hallquist. LS-DYNA Theory Manual 971 rev5-beta, Livermore Software Technology Corporation, 2010

[2] Markus Brede, Methodenentwicklung zur Berechnung von höherfesten Stahlklebeverbindungen des Fahrzeugbaus unter Crashbelastung, Forschung für die Praxis P 676, Forschungsvereinigung Stahlanwendungen e.V. im Stahl-Zentrum, 2008

[3] Frank Burbulla Anton Matzenmiller. Kontinuumsmechanische Modellierung von Stahlblechklebeverbindungen für die FE-Crashanalyse. 7. LS-DYNA Anwenderforum, Bamberg, 2008

[4] Markus Brede, Felix Kleiner, Stephan Marzi, Olaf Hesebeck. A rate-dependent, elasto-plastic cohesive zone mixed-mode model for crash analysis of adhesively bonded joints. 7th European LS_DYNA Conferenc, 2009.

[5] P. Davies A.J. Brunner, B.R.K. Blackman. A status report on delamination resistance testing of polymer-matrix composites. Engineering Fracture Mechanics 75, 2008, page 2779–2794

[6] Pedro P. Camanho. Mixed-mode decohesion finite elements for the simulation of delamination in composite materials. Carlos G. Dávila Langley Research Center-Hampton, Virginia, Technical Memorandum NASA/TM-2002-2117737, 2002

[7] Anton Matzenmiller, Mark Fiolka. Berechnung fortschreitender Risse in Laminaten. 23rd CADFEM Users' Meeting 2005, International Congress on FEM Technology with ANSYS CFX & ICEM CFD Conference, 2005.

[8] Nielen Stander Willem Roux Tushar Goel Trent Eggleston Ken Cralg, LS-OPT® User's Manual, a design optimization and probabilistic analysis tool for the engineering analyst, Livermore Software Technology Corporation, Version 4.2, 2012

[9] J. Costa C.G. Da´vila A. Turon, P.P. Camanho. A damage model for the simulation of delamination in advanced composites under variable-mode loading, Volume 38, Issue 11, 2006, Pages 1072-1089

[10] Japanese Industrial Standard, Testing methods for interlaminar fracture toughness of carbon fiber reinforced plastic, JIS K 7086-1993